

Immune microenvironment heterogeneity reveals distinct subtypes in neuroblastoma: insights into prognosis and therapeutic targets

Yanlan Yang^{1,*}, Huamei Li^{2,*}, Donghui Zheng¹, Xuemei Li¹, Hongyan Liu¹

¹Department of Hematology and Oncology, Shenzhen Children's Hospital, Shenzhen, Guangdong, PR China

²Department of Hepatobiliary Surgery, The Affiliated Drum Tower Hospital, Medical School, Nanjing University, Nanjing 210008, PR China

*Equal contribution

Correspondence to: Xuemei Li, Hongyan Liu; **email:** 220191952@seu.edu.cn, 230179525@seu.edu.cn

Keywords: neuroblastoma, tumor microenvironment, subtypes, prognosis, drug response

Received: July 11, 2023

Accepted: October 23, 2023

Published: November 27, 2023

Copyright: © 2023 Yang et al. This is an open access article distributed under the terms of the [Creative Commons Attribution License](https://creativecommons.org/licenses/by/4.0/) (CC BY 4.0), which permits unrestricted use, distribution, and reproduction in any medium, provided the original author and source are credited.

ABSTRACT

Background: Neuroblastoma (NB) is a childhood cancer originating from immature nerve cells in the sympathetic nervous system. Current clinical and molecular subtyping methods for NB have limitations in providing accurate prognostic information and guiding treatment decisions.

Results: To overcome these challenges, we explored the microenvironment of NB based on the knowledge-based functional gene expression signatures (Fges), which revealed heterogeneous subtypes. Consensus clustering of Fges activity scores identified three subtypes (Cluster 1, Cluster 2, and Cluster 3) that demonstrated significant differences in prognosis compared to mainstream subtypes. We assessed the immune infiltration, immunogenicity, CD8T cytotoxicity, and tumor purity of these subtypes, uncovering their distinct biological functions. Cluster 1 and Cluster 2 exhibited higher immunoreactivity, while Cluster 3 displayed higher tumor purity and poor prognosis. Gene ontology annotation and pathway analysis identified immune activation in Cluster 1, epithelial-mesenchymal transition (EMT) in Cluster 2, and cell cycle processes in Cluster 3. Notably, the impact of EMT activity on prognosis may vary across NB subtypes. A classification model using XGBoost accurately predicted subtypes in independent NB cohorts, with significant prognostic differences. *GPR125*, *CDK4*, and *GREB1* emerged as potential therapeutic targets in Cluster 3. *CD4K* inhibitors showed subtype-specific responses, suggesting tailored treatment strategies. Single-cell analysis highlighted unfavorable clinical features in Cluster 3, including high-risk classification and reduced cytotoxicity. Suppressed interactions between monocytes, macrophages, and regulatory T cells were observed, affecting immune regulation and patient prognosis.

Conclusion: To summarize, we have identified a new independent prognostic factor in NB that underscores the significant correlation between tumor phenotype and immune contexture. These findings deepen our understanding of NB subtypes and immune cell interactions, paving the way for more effective treatment approaches.

INTRODUCTION

Neuroblastoma (NB) is a childhood cancer that originates from the neural crest during embryonic development and

primarily occurs in the sympathetic nervous system [1]. Common symptoms include the presence of an abdominal mass, discomfort, and swelling, along with ocular changes, bone pain, fever, fatigue, and irritability.

Early diagnosis and treatment are crucial for improving the prognosis in children with this condition. Clinically, diagnosing NB involves both laboratory tests and imaging. Laboratory tests check for specific substances like Vanillylmandelic acid/Homovanillic acid (VMA/HVA) in urine, blood, and bone marrow. Imaging techniques include ultrasound, computed tomography (CT) scans, magnetic resonance imaging (MRI), metaiodobenzyl-guanidine (MIBG) scans, bone scans, and positron emission tomography (PET)-CT scans. These tools are crucial for accurately diagnosing NB, determining its stage, and planning the appropriate treatment. In terms of the affected population, NB is most commonly diagnosed in young children, with a slight male predominance, affecting individuals of all racial backgrounds. Notably, Black and Native American patients with NB tend to have a higher incidence of high-risk disease, leading to poorer Event-Free Survival (EFS) outcomes compared to white patients [2, 3]. In particular, due to the variability in clinical presentation and disease progression, 5-year survival rates for NB show considerable diversity. Research studies indicate that the 5-year survival rate for NB is below 50% [4, 5].

Considering the heterogeneous nature of NB, patient-specific staging to address different treatment strategies is clinically relevant. Currently, three primary approaches for staging and classifying NB are commonly employed: The International Neuroblastoma Staging System (INSS), the International Neuroblastoma Risk Group (INRG), and the Children's Oncology Group (COG) risk stratification [6, 7]. The INSS classification categorizes tumors into four stages based on their size, depth, and aggressiveness to forecast patient prognosis and formulate treatment plans. INRG classifies patients into low, medium, and high-risk groups. Low-risk patients may not require immediate treatment, whereas medium-risk individuals often undergo a combination of chemotherapy, surgery, and radiation. High-risk cases, the most severe, demand intensive treatment, involving potent strong chemotherapy, surgery, radiation, immunotherapy, and stem cell transplants [8]. Conversely, COG risk stratification relies on the biological and molecular genetic traits of the tumor to devise treatment strategies and assess prognosis [6, 7, 9]. Additionally, there are supplementary molecular subtyping techniques applicable to NB, encompassing classifications related to chromosomal ploidy and groupings contingent on mutational conditions [10–13]. In the context of high-risk NB patients, a significant frequency of genetic variances is observed within specific chromosomal regions, specifically 1p, 11q, and 17q. Specifically, the presence of 11q deletion in NB cases without *MYCN* amplification, often indicates a highly malignant form with an unfavorable prognosis [14, 15]. Familial NB is associated with mutations in

the *PHOX2B* and *ALK* genes, which can be inherited and are frequently accompanied by other syndromes related to neurocognitive development [16, 17]. High-risk NB patients often exhibit elevated levels of *BDNF* and *TrkB*, correlating with the malignancy and poor prognosis [18]. Alterations in the RAS and p53 pathway genes are commonly observed in high-risk and recurrent NB cases. *SETD8*, a histone methyltransferase, may be associated with a poor prognosis in *MYCN* non-amplified NB [19]. Additionally, the *BARD1* gene and its isoform protein, *BARD1β*, are linked to high-risk NB and could potentially serve as therapeutic targets [20]. *DDX1* and *DDX4* have also been identified in specific NB cases, exhibiting associations with distinct disease characteristics [21]. Nevertheless, further research is essential for gaining a comprehensive understanding of their functions and clinical significance. Furthermore, mutations and deletions in *ARID1A/B* have been correlated with drug resistance and elevated mortality rates in NB, indicating the potential pivotal roles of these genes in NB development [22]. Notably, HVA and VMA are breakdown products of dopamine and are useful for diagnosing NB. Elevated ferritin, lactate dehydrogenase (LDH), and neuron-specific enolase (NSE) levels are associated with NB, helping in diagnosis, assessing disease extent, and predicting prognosis. When considered alongside clinical and imaging findings, these biomarkers offer valuable insights into NB's status and progression.

Although the acceptance of genomic analysis in clinical decision-making is on the rise, current classification systems and biomarkers also have limitations in accurately portraying the biological and molecular genetic characteristics of tumors, hindering the development of personalized treatment plans and precise prognostic assessments [23]. Therefore, the introduction of a new classification strategy for NB is highly anticipated. Recently, transcriptome analysis provides a deeper understanding of tumor complexity and heterogeneity, presenting an opportunity to discover new biomarkers for the development of innovative treatment strategies [24]. The tumor microenvironment (TME) plays a pivotal role in clinical outcomes and treatment response. Immune cells infiltrating the tumor can profoundly impact tumor progression and the success of cancer therapy by exerting both pro- and anti-cancer effects [25, 26]. Researches have been demonstrated that cancer-associated fibroblasts (CAFs) and vascular signaling of stromal cells can impact outcomes [24, 27]. Therefore, deciphering the tumor immune microenvironment profile can enhance individualized targeted and immunotherapy strategies. Notably, computational methodologies are particularly essential in oncology, enabling the discovery of novel diagnostic, prognostic, and treatment agents. These

techniques leverage complex biological data and extensive datasets to identify molecular signatures associated with various cancer types, improving early and precise cancer diagnostics. Furthermore, they assist in modeling cancer progression, predicting patient outcomes, and refining personalized treatment approaches through data-driven analyses and machine learning [28–31]. At present, the investigation of NB subtypes through immune microenvironment transcriptomic features is ongoing, the integration of computational methodologies and transcriptome data plays a crucial role in understanding the heterogeneity of the NB microenvironment.

In our research, based on the knowledge-based functional gene expression signatures (Fges) provided by Bagaev et al. [24], which reflect the major functional components of TME, we systematically investigated the activity of these gene sets in NB patients and their association with prognosis based on the computational strategy. By utilizing the activity of Fges, we effectively identified NB patients into three distinct subtypes and explored the molecular features and functional heterogeneity in the microenvironment. To ensure generalization to other NB patient cohorts, we have developed a reliable classification model, and combined with drug sensitivity analysis, provides potential clinical guidance for treatment. Specifically, our study focused on utilizing single-cell expression profiles to uncover the key molecular mechanisms that contribute to the prognostic differences observed among NB subtypes.

MATERIALS AND METHODS

Data source and preprocessing

In the present study, we obtained transcriptome sequencing expression data and clinical data for NB patients from “Therapeutically Applicable Research to Generate Effective Treatments” (TARGET) database (named TARGET-NB cohort, $n = 151$), with expression data normalized by FPKM (Fragments Per Kilobase of exon model per Million mapped fragments). TARGET-NB cohort data were mainly used to explore TME and as the training data for investigating the potential subtypes of NB. Also, GSE49710 ($n = 357$) [32–34] and GSE85047 ($n = 266$) [35] cohorts from the Gene Expression Omnibus (GEO) accessed using “GEOquery” (version 2.60.0) [36], and clinical data corresponding to these two datasets were also acquired. Background correction and quantile normalization were performed using *rma* function from “affy” package (version 1.70.0) [37] for expression data, and combined with clinical data to evaluate the prognosis performance of derived

novel NB subtypes. More detailed information can be found in Supplementary Table 1.

To investigate the intrinsic molecular mechanisms of heterogeneity in NB subtypes, we further obtained a single-cell dataset provided by Verhoeven et al. [5] from <https://github.com/shenglinmei/NB.immune.atlas/>. This dataset includes 46,134 cells from 17 NB patients and covers ten major immune cell types, including B cells, ILC3, Macrophages, mDC, Monocytes, NK cells, Plasma cells, Cytotoxic T cells (Tcyto), Helper T cells (Th), and Regulatory T (Treg) cells.

Gene set activity score and signature score

We used the GSVA package (version 1.40.1) [38] with the “method = gsva” to examine the activity score of given gene sets for NB patients. The signature scores of a list of gene sets were evaluated using the *AddModuleScore* function from the Seurat package.

Consensus clustering for investigating potential subtypes of NB

To investigate the potential molecular subtypes of NB, we obtained 29 cell types closely associated with the TME and their corresponding signature genes from https://github.com/BostonGene/MFP/blob/master/signatures/gene_signatures.gmt (Supplementary Table 2). We used the “ssgsea” method in the GSVA package to assess the activity of these cell types in NB patients, transforming the gene expression matrix into an activity score matrix for different cell types in the microenvironment. In this matrix, rows represent cell types, columns represent samples, and each entry represents an activity score. Based on this activity matrix, we utilized unsupervised consensus clustering, implemented by the “ConsensusClusterPlus” R package (version 1.62.0) [39] with parameters “clusterAlg = pam, distance = pearson, pItem = 0.8”, to derive intrinsic subtypes of NB in the TARGET-NB cohort. In the present study, we determined the optimal number of clusters by varying the number from 2 to 6 and selecting the most stable consensus matrices and unambiguous cluster assignments across permuted clustering runs.

Kaplan-Meier survival curve

Kaplan-Meier (KM) survival analysis, along with the log-rank test, was used to determine if the subtypes showed a significantly different overall survival (OS). For gene expression data, the optimal cutoff point for group stratification was determined using the *surv_cutpoint* function in the “survminer” package (version 0.4.9) [40]. Statistical significance was determined by a *p*-value less than 0.05.

Differentially expressed genes (DEGs) associated with the Fges-derived subtypes

To identify DEGs across subtypes, we utilized the *FindAllMarkers* function from “Seurat” package (version 4.3.0) [41]. Specifically, genes with adjusted *p*-values below 0.01 and an absolute log₂FC greater than 1 were deemed significantly differentially expressed.

Functional enrichment analysis

To examine the distinct biological processes and pathways that exhibited significant differential expression among subtypes, we employed the “clusterProfiler” package (version 4.0.5) [42] to convert gene symbols into Entrez ids using the *bitr* function. Subsequently, gene ontology (GO) and KEGG pathway enrichment analysis was conducted using the *enrichGO* function with the “ont = BP” parameter and *enrichKEGG* function, respectively. GO and KEGG terms that had adjusted *p*-values below 0.01 were regarded as significantly enriched.

Estimation of tumor purity, immune score, immunophenoscore, and cytotoxicity score

The estimation of immune score, and tumor purity of NB patients was conducted by utilizing the “ESTIMATE” package (version 1.0.13) [43], as specified in the official manual. The Immunophenoscore (IPS) employs various markers of immune response or immune tolerance to measure the immune activity within an NB patient. A higher score of IPS indicates a greater level of immunogenicity [44]. The cytotoxicity score for each NB patient was determined by utilizing GSVA tool with *GZMA* and *PRF1* markers [45].

Prediction of Cluster 1&2 and Cluster 3 subtypes for NB patients

Given that the Cluster 3 identified by the TARGET-NB cohort demonstrated the worst prognosis, we introduced the XGBoost model [30] to distinguish between Cluster 1&2 and Cluster 3 categories for individual NB patients. The following steps were taken: (1) The TARGET-NB cohort was randomly split into training and testing sets at a 3:1 ratio. We used the “FindAllMarkers” function from the Seurat package to identify genes that were significantly different in the Cluster 1&2 and Cluster 3 groups (adjusted *p*-value ≤ 0.01) as the features for the training set. (2) We applied the XGBoost model to the training set using 10-fold cross-validation, as implemented by the “xgb.cv” function from the “xgboost” R package (version 1.6.0.1). The parameters used were “nfold = 10, objective = multi:softprob,

max.depth = 10, eval_metric = mlogloss” [46]. The model with the highest area under the curve (AUC) value was retained, and its performance was further evaluated using the testing set and two independent cohorts (GSE49710 [32–34] and GSE85047 [35]).

Significance of novel NB subtypes in drug sensitivity

To assess the drug sensitivity of the Cluster 1&2 and Cluster 3, we utilized the “oncoPredict” package (version 0.2) [47] with the “batchCorrect = eb” parameter to determine the half-maximal inhibitory concentration (IC₅₀) values of Palbociclib and Ribociclib anti-tumor drugs for the three cohorts of NB, respectively. This package employs a gene expression and drug sensitivity modeling algorithm for cell lines in the Cancer Genome Project, with the aim of predicting clinical chemotherapeutic response.

Cell-cell interactions analysis

We employed CellChat [48] (version 1.6.1) to determine cell-cell interactions based on the expression of known ligand-receptor (L-R) pairs in different cell types. Briefly, the input for CellChat consisted of gene expression data of cells along with their assigned cell types. Initially, we identified overexpressed ligands or receptors within specific cell groups and projected the gene expression data onto a protein-protein interaction network. Overexpressed L-R interactions were identified when either the ligand or the receptor was overexpressed. Subsequently, CellChat facilitated the inference of biologically significant cell-cell communication by assigning a probability value to each interaction and conducting a permutation test. Finally, the resulting communication networks were visualized using a circle plot, and the signaling pathways were visualized using a bubble plot.

Statistical analysis

The study utilized standard statistical tests such as Student’s *t*-test, Wilcoxon rank-sum test, log-rank test, and Cox proportional hazards regression to analyze both clinical and expression data. These analyses were carried out using R4.2.2.

Availability of data and material

We collected gene expression data and corresponding clinical information for the NB cohorts from publicly available databases, as outlined in Supplementary Table 1. Especially, for this study, we utilized R 4.2.2 for the analysis, and the relevant R packages are described in detail in the Materials and Methods section. All codes are available upon request to the corresponding author.

RESULTS

Fges portray the heterogeneity of the TME in NB patients and the strong association with prognosis

To investigate the TME of NB, we utilized a transcriptomic-based analytical platform and selected 29 functional gene sets (Fges) that represented the major functional components of the tumor, as well as immune, stromal, and other cell populations from previous study [24] (Supplementary Tables 1 and 2). We then employed GSVA (method = "ssgsea") to assess the activity score of Fges in TARGET-NB patients, and found that the distribution of scores varied across patients, indicating the heterogeneous TME in NB patients (Figure 1A; Supplementary Table 3; see Materials and Methods). Interestingly, patients within the blue dashed box, showed a high degree of homogeneity in the distribution of activity scores, suggesting the presence of distinct subtypes in the microenvironment of NB (Figure 1A). We raised the question of whether the mainstream classifications could explain the heterogeneity in the microenvironment of NB patients. To investigate this, we analyzed the Fges score in COG risk categories, and found that, except for Protumor_cytokines, Coactivation_molecules, B_cells, Effector_cells, T_cells, Th1_signature, and T_cell_traffic, most (22/29) of Fges were no significant differences among low, intermediate, and high-risk categories under p -value ≤ 0.01 . This suggests that COG risk stratification may not fully reflect the changes in the microenvironment of NB (Figure 1B). Also, we examined differences in Fges score across INSS stages and box plots showed that, similar to COG risk subtypes, most Fges (26/29) did not show significant differences. However, nearly half (13/29) of the Fges exhibited significant differences in *MYCN* status (amplified or not amplified), suggesting that the subtypes portrayed by *MYCN* may be more closely linked to the TME of NB (Figure 1B). Notably, we observed no Fges that shared significant differences in COG, INNS and *MYCN* (Figure 1B).

We also analyzed the interactions between Fges and their prognostic implications, showing that most Fges were synergistic in the NB microenvironment, such as MHC II and Macrophage_DC_traffic (Figure 1C; Supplementary Table 4; see Materials and Methods). The MHC II molecule is involved in promoting T-cell activation and clearance of tumor cells. In NB patients, higher levels of MHC II expression are associated with longer survival (Figure 1C). Similarly, increased expression of Macrophage_DC_traffic, a gene signature related to immune cell infiltration, is also a predictor of better prognosis in NB (Figure 1C). Typically, T_reg and T_reg_traffic hinder the immune

response against tumors and their high levels are frequently linked to poor prognosis. However, our observations indicate that these two factors actually have a significant favorable impact on the prognosis of NB patients, suggesting the complexity and heterogeneity of NB patients. On the other hand, Proliferation_rate is a major risk factor, as a high proliferation rate suggests that the tumor has a greater growth capacity, faster growth rate, and higher malignancy level.

To sum up, the activity of Fges is responsive to the microenvironment heterogeneity in NB patients and is closely associated with prognosis. These findings have the potential to improve our understanding of NB tumor mechanisms and to guide the development of new classification strategies.

Derivation of novel subtypes associated with distinct microenvironmental characteristics of NB from the perspective of Fges

To investigate if functional gene sets (Fges) can reveal molecular subtypes of NB, distinct from those identified previously based on clinical and molecular features, we conducted a consensus clustering analysis on the activity scores of Fges, resulting in the categorization of patients into three subtypes: Cluster 1, Cluster 2, and Cluster 3 (Figure 2A; Supplementary Table 3). We first examined the sample sizes of the three new subtypes, with Cluster 1 having the highest number of samples ($n = 61$) and Cluster 2 the lowest ($n = 40$), with a more evenly distributed overall distribution (Figure 2A; Supplementary Table 5; see Materials and Methods). Moreover, significant differences in the prognosis of these three subtypes were observed, with Cluster 2 showing the best prognosis, followed by Cluster 1, and Cluster 3 having the worst (Figure 2B; see Materials and Methods). Furthermore, we analyzed the distribution of Fges activity scores in the three subtypes, and revealed significant differences in all functional gene sets. Interestingly, Cluster 3 showed the lowest overall activity scores, while EMT_signature, Matrix, and CAF showed higher activity scores in Cluster 2, suggesting that EMT may help to inhibit the growth and spread of NB tumors, leading to a better prognosis (Figure 2C). We also found that immune cells, such as T_cells and effector_cells exhibited high activity scores in Cluster 1, but their prognosis was slightly worse than that of Cluster 2, suggesting that high degree of immune infiltration in this subtype may indicate that the tumor or infection is suppressing the immune system, leading to a poorer prognosis for patients (Figure 2C).

By comparing the associations between the three subtypes and other clinical features and classical staging, including gender, COG, survival status, and

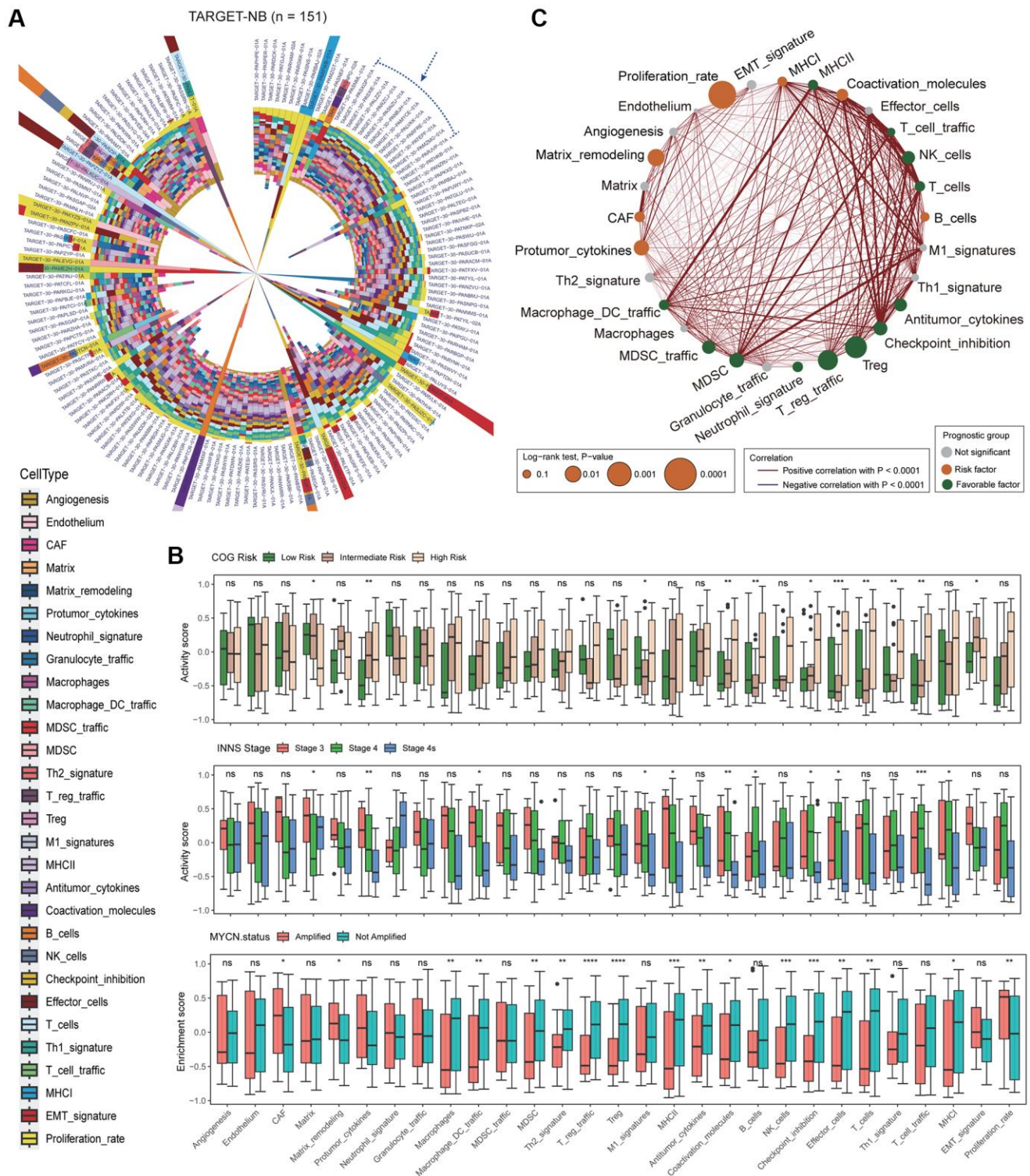


Figure 1. Analysis of Fges activity scores reveals the heterogeneity of the neuroblastoma microenvironment and its significant impact on prognosis. (A) Circular stacked bar plot shows the distribution of activity scores of 29 Fges in TARGET-NB patients. Different colors represent different gene sets (Supplementary Tables 2 and 3). (B) Box plot shows the distribution of activity scores of Fges in TARGET-NB patients in different groups, with p -values obtained by Wilcoxon rank-sum test. Abbreviation: ns: not significant; * $p < 0.05$; ** $p < 0.01$; *** $p < 0.001$; **** $p < 0.0001$. (top panel) COG risk groups; (middle panel) INNS stages; (bottom panel) *MYCN* amplified or not. (C) Network plot displays the interaction of Fges within the microenvironment of NB and their influence on the prognosis of patients. Positive Pearson correlations between sets of genes are represented by red lines, while significant negative associations are denoted by blue lines. The significance of each gene set in predicting the prognosis of NB patients is depicted by the size of the corresponding circle. Gene sets that have a protective effect are shown in green, while those that pose a risk are represented in red; otherwise, they are shown in gray.

INSS stages, we found that Cluster 3 was more likely to occur in males and had higher mortality rates (Figure 2D). However, we also noticed that Cluster 1,

Cluster 2, and Cluster 3 did not differ significantly in COG risk groups as well as INSS stages, suggesting inherent differences between the subtyping identified by

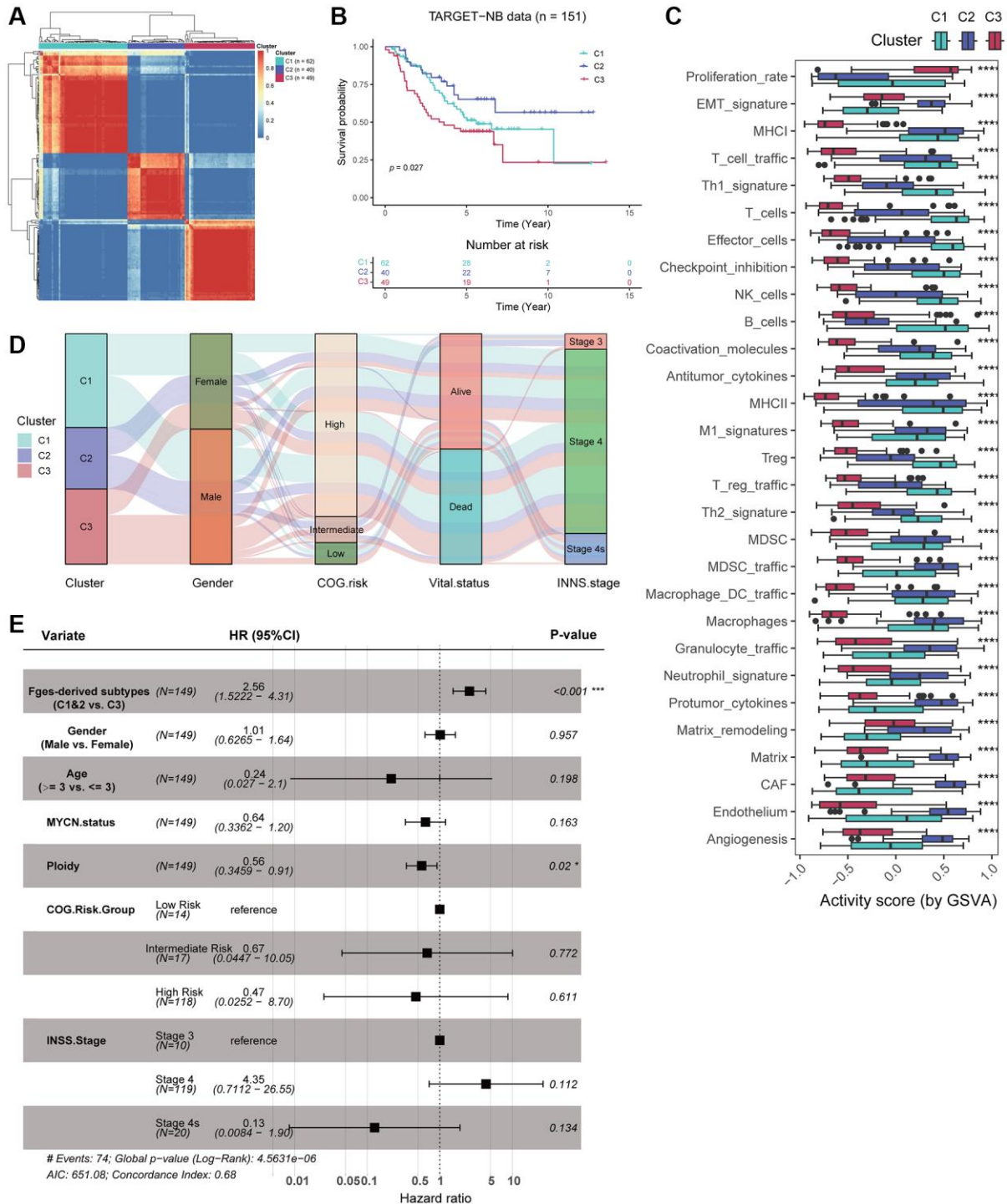


Figure 2. Consensus clustering identified three novel subtypes based on Fges activity scores. (A) Heatmap shows the consensus clustering matrix of the TARGET-NB cohort based on the activity score of Fges. **(B)** KM curve shows that the three Fges-derived subtypes exhibit significant differences in prognosis. *P*-value was obtained by log-rank test. **(C)** Box plot shows the distribution of activity scores of Fges in three Fges-derived subtypes. *P*-value was obtained by Wilcoxon rank-sum test. *****p* < 0.0001. **(D)** Sankey plot shows the associations between the Fges-derived subtypes and clinical features, including gender, COG risk groups, survival status, and INSS stages. **(E)** Forest plot shows the independent effect of Fges-derived subtypes, along with other clinical features as well as classical groupings, on the prognosis of patients with neuroblastoma. This was determined through multivariate Cox regression analysis.

Fges and COG as well as INNS (Figure 2D). Moreover, to determine whether Fges-derived subtyping could be used as an independent prognostic risk factor in clinical studies of NB, we employed multiple Cox regression with covariates including Fges-derived subtypes, Gender, Age, *MYCN*, Ploidy, COG, and INSS (Figure 2E). The results indicated that Cluster 3 was a significant risk factor relative to Cluster 1 and Cluster 2, and there was no significant effect on prognosis except for Ploidy, suggesting that Fges-derived NB subtypes is an independent prognostic factor and has a good advantage in distinguishing prognosis significantly compared to other clinical characteristics and typing strategies (Figure 2E).

Biological differences across Fges-derived NB subtypes

Next, we investigated the activity score of cancer hallmark pathways collected from MSigDB in three Fges-derived subtypes using “ssGSEA” method, and hierarchical clustering clearly showed that these pathways could form two distinct categories (Figure 3A; see Materials and Methods). One category (i.e., H1) had a higher level of activity in Cluster 1 and Cluster 2, which are potential protective factors in NB patients, while the other category (i.e., H2) had a higher level of activity in Cluster 3, indicating risk factors (Figure 3A). To validate this finding, we selected two cancer hallmark pathways from each category, including HALLMARK_ALLOGRAFT_REJECTION, HALLMARK_IL6_JAK_STAT3_SIGNALING, HALLMARK_UV_RESPONSE_UP, and HALLMARK_IL2_STAT5_SIGNALING, and observed their KM curves of OS. The results showed that high activity in Cluster 3 for HALLMARK_ALLOGRAFT_REJECTION and HALLMARK_IL6_JAK_STAT3_SIGNALING exhibited a significantly worse prognosis, while high activity in HALLMARK_UV_RESPONSE_UP and a higher degree of activity in HALLMARK_IL2_STAT5_SIGNALING (Clusters 1&2) predicted a better prognosis, consistent with our previous inference (Figure 3B). Overall, these analyses suggest that hallmark pathways highly relevant to tumor progression exhibit distinct roles and patterns in Fges-derived subtypes.

Moreover, we delved deeper into the biological diversity among the three Fges-derived subtypes, encompassing immune infiltration, tumor purity, IPS, and cytotoxicity. The findings revealed that Clusters 1&2 displayed substantially higher (*t*-test, *p*-value ≤ 0.01) immune infiltration, immunogenicity and cytotoxicity scores, while Cluster 3 exhibited significantly lower immune infiltration and the greatest level of tumor purity (Figure 3C; see Materials and Methods). To reinforce these results, we also evaluated

the activity of 28 immune cell types (782 marker genes) obtained from Charoentong P et al. [44] within the three subtypes and demonstrated that Clusters 1&2 had a greater degree of immunity in comparison to Cluster 3 (Figure 3D; see Materials and Methods). These analyses suggest that elevated immune infiltration is strongly linked to a favorable prognosis, indicating that NB is a “hot” tumor, consistent with prior investigations [49, 50].

To elucidate the biological functions and pathways involved in the three Fges-derived subtypes, we conducted differential gene expression analysis. This revealed that T cell and B cell markers such as *CD3D*, *CD3E*, *CD19*, and *CD79A* were highly expressed in Cluster 1, while fibroblast-related genes such as *DCN* and *CDH19* were highly expressed in Cluster 2 (Figure 3E; Supplementary Table 6). Additionally, genes associated with meiosis, including *MND1*, *NCAPG*, and *BUB1*, were significantly highly expressed in Cluster 3 (Figure 3E; Supplementary Table 6). Further functional enrichment analysis showed that Cluster 1 was associated with immune response processes and T-cell activation pathways, Cluster 2 was significantly associated with extracellular matrix organization and ECM-receptor interactions, and Cluster 3 was significantly associated with the cell cycle, indicated that the Fges-derived isoforms exhibit significant biological heterogeneity (Figure 3F, 3G; Supplementary Table 7; see Materials and Methods).

Predicting Fges-derived subtypes with XGBoost model

Our objective was to develop a precise and sensitive method for predicting patient Fges-derived subtypes without relying on unsupervised clustering. To achieve this goal, we utilized the TARGET-NB cohort and trained our model using the XGBoost algorithm to predict Cluster 1&2 and Cluster 3 subtypes (Figure 4A; see Materials and Methods). Using differential gene expression analysis, we identified a set of genes that were able to predict whether a sample belonged to Cluster 3 with high sensitivity and specificity (Supplementary Table 8). We then integrated these genes into our XGBoost model for training. Our model achieved an accuracy of 0.953 (0.906–0.981) in predicting subtypes (Figure 4B; see Materials and Methods). We observed that 93.6% of samples assigned to Clusters 1&2 by clustering were predicted to be 1&2 by our model, while 85.7% of samples assigned to Cluster 3 through clustering were found in Cluster 3 (Figure 4B). By applying our model to two other NB testing cohorts GSE49710 and GSE85047, and combining it with clinical information, we were able to

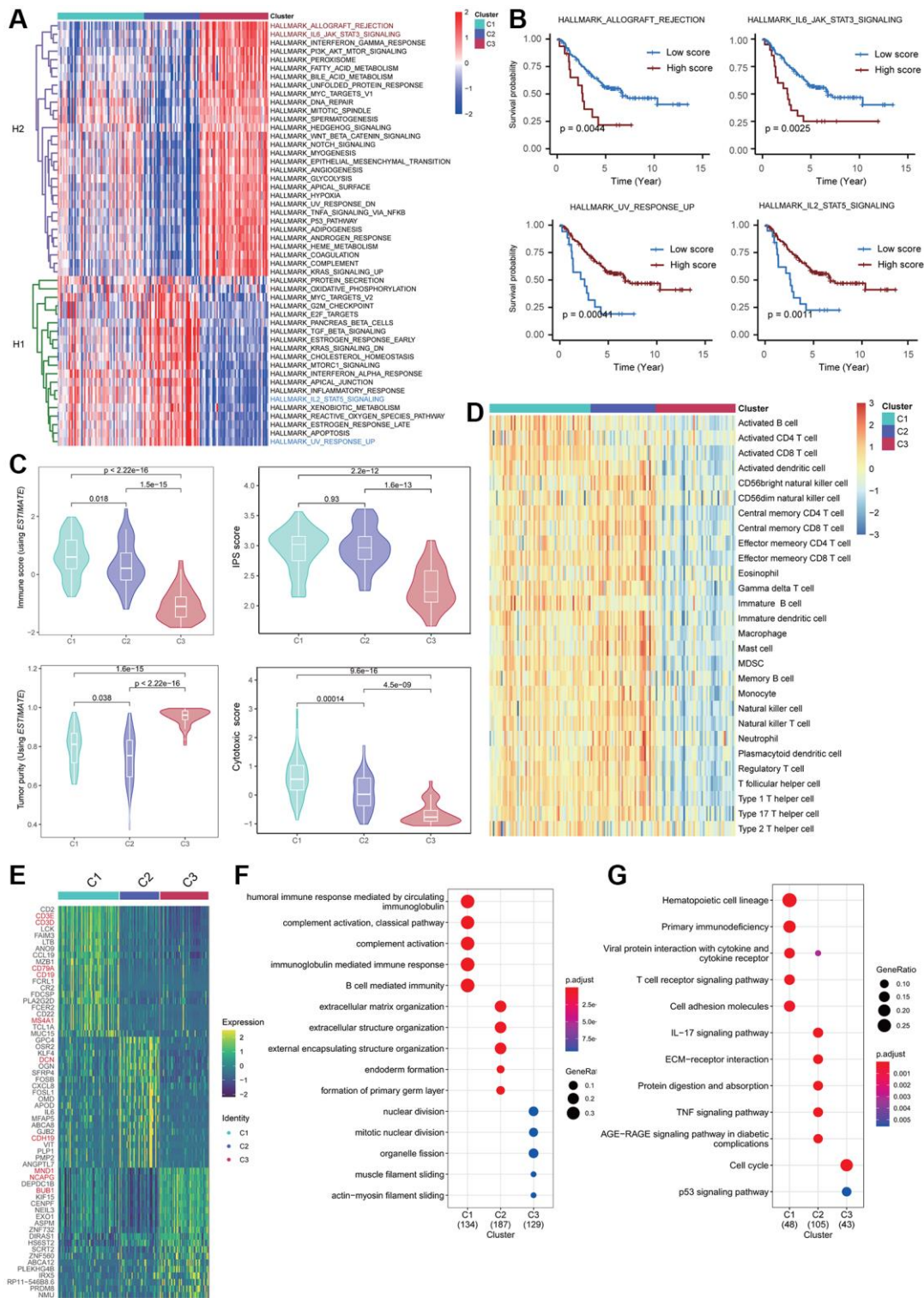


Figure 3. Biological heterogeneity across Fges-derived subtypes. (A) Heatmap displays the activity scores of cancer hallmark pathways for Cluster 1, Cluster 2, and Cluster 3 subtypes. These pathways were collected from MSigDB database, and can be classified into two categories, H1 and H2. (B) KM curves demonstrate the significant impact of high activity in the four cancer hallmark pathways on the prognosis of NB patients. The p -values were obtained through log-rank tests. (C) Violin plots show the distribution of different biological features in the three Fges-derived subtypes, including immune score, IPS, tumor purity, and cytotoxic score. P -values were obtained by a t -test. (D) Heatmap of activity scores of 28 immune cell gene sets provided by a previous study [44], among the Fges-derived subtypes. (E) Heatmap shows the expression of the top 20 highly expressed genes among three Fges-derived subtypes. (F) Bubble plot shows the biological processes significantly involved in the three Fges-derived subtypes of NB. (G) Bubble plot shows the pathways significantly involved in the three Fges-derived subtypes of NB.

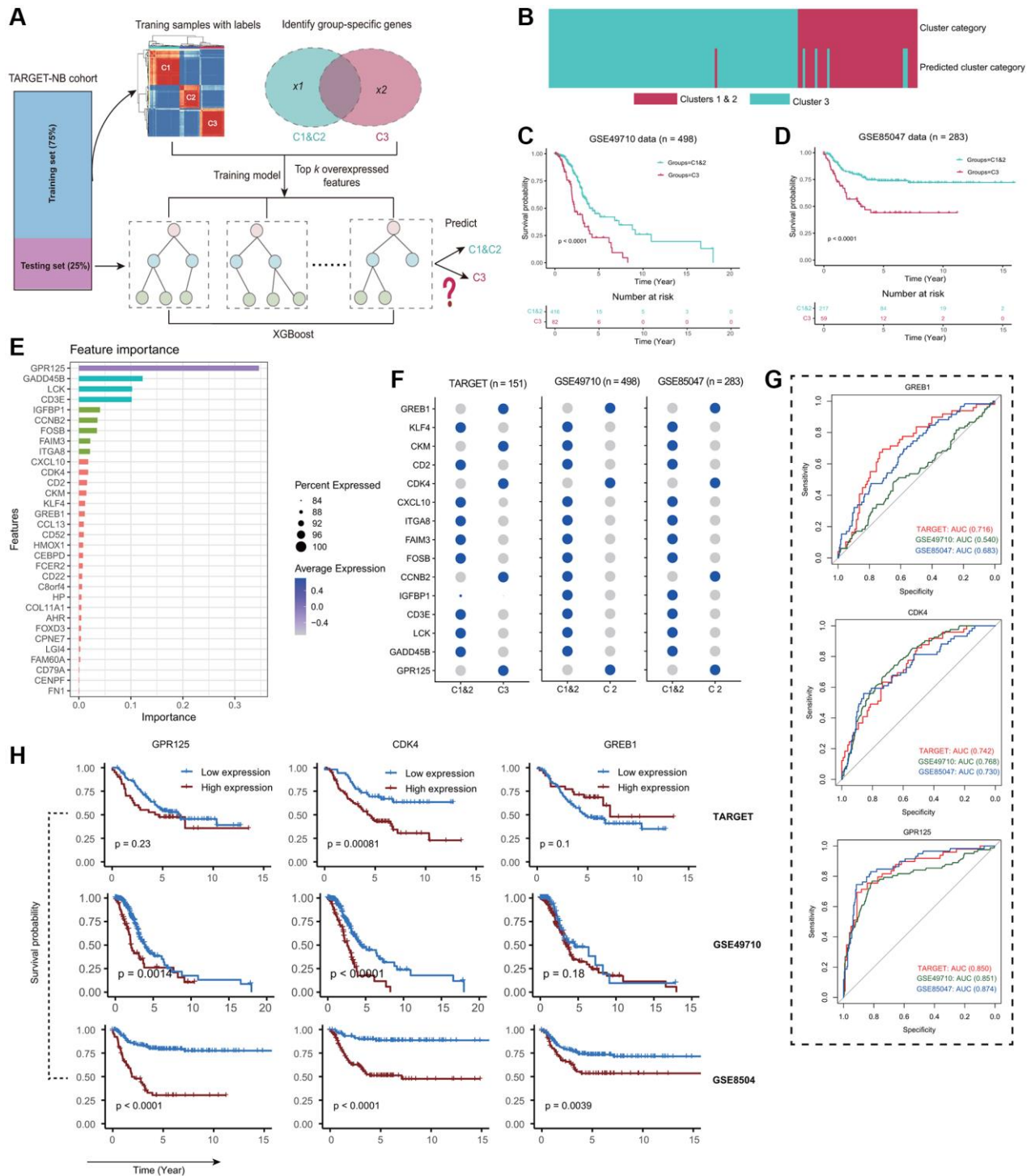


Figure 4. Independent datasets validation of the reliability of Fges-derived subtypes. (A) Schematic of the XGBoost model for predicting Fges-derived subtypes (see Materials and Methods). (B) Heatmap shows whether a particular sample, predicted by XGBoost classifier from the training set, falls under Cluster 3 (light blue) or Cluster 1&2 (purple), out of the 151 total samples. (C, D) The association between predicted clusters and survival was tested using Kaplan-Meier survival curves for predicted Cluster 3 versus Cluster 1&2. P -values were from log-rank tests. (E) Bar plot shows the importance ranking of the top 35 feature genes (ordered by Gain index) filtered by XGBoost in the training set. (F) Bubble plots show the expression of the top 15 important feature genes in the three NB cohorts. The depth of the color indicates the average level of expression of one gene in a particular subtype, and the size of the circle indicates the percentage of that gene expressed in a particular subtype. (G) ROC curves depict how accurately the expression of three genes can predict subtypes Cluster 1&2 in comparison to Cluster 3 based on the TARGET-NB cohort. (top) *GREB1*; (middle) *CDK4*; (bottom) *GPR125*. (H) KM curves show the prognostic impact of high and low expression of *GREB1*, *CDK4* and *GPR125* genes in three NB cohorts. (top panel) TARGET-NB; (middle panel) GSE49710; and (bottom panel) GSE85047.

demonstrate significant differences in prognosis for Cluster 1&2 and Cluster 3 subtypes (Figure 4C, 4D). These results were consistent with our observations in the TARGET-NB cohort, which suggests that Fges-derived subtypes are highly consistent across NB cohorts. In summary, our XGBoost model refined Cluster 3 and provided a single-sample predictor that can be used for every patient in the clinic.

Next, we analyzed the importance of feature genes in our XGBoost prediction model and found that *GPR125* had the highest importance (Figure 4E). Previous studies have confirmed that this gene plays a crucial role in the development of the nervous system and is involved in the migration and differentiation of neural stem cells, indicating that *GPR125* is a vital biomarker for the clinical study of Cluster 3 [51–53]. Additionally, we observed the expression of these significant signature genes and found that *GREB1*, *CDK4*, and *GPR125* showed highly consistent expression in Cluster 3 of the three NB cohorts, with *CDK4* and *GPR125* predicting an AUC of greater than 0.7 for Cluster 1&2 and Cluster 3 in all three NB cohorts, implying good discriminatory ability (Figure 4F, 4G). Interestingly, in combination with clinical information, we found that *CDK4* performed best in predicting the prognosis of patients in three NB cohorts, which is an essential tumor driver gene and may be a crucial prognostic marker for the Cluster 3 (Figure 4H) [54–56]. In conclusion, by analyzing multiple perspectives, we found that *GREB1*, *CDK4*, and *GPR125* may be the critical markers of Cluster 3 in NB, especially *CDK4* and *GPR125*. Clinically, by suppressing the expression of these genes, it may have important to improve prognosis for NB patients.

Drug sensitivity assessment for Fges-derived subtypes

Considering the potential clinical application of *CDK4* in Fges-derived Cluster 3, we used GeneMANIA to construct a protein-protein interaction network and identify genes associated with *CDK4*. The results showed that *CDK4* is involved in cell cycle as well as regulatory activities (Figure 5A). This finding further suggests that high expression of this gene promotes the proliferation of tumor cells. Currently, *CDK4*-targeted drug inhibitors are an emerging approach to cancer treatment, with several drugs already approved by the Food and Drug Administration (FDA) and showing good efficacy in clinical practice. For example, Palbociclib [57, 58] can halt tumor cell proliferation by inhibiting the G1/S phase transition of the cell cycle, while Ribociclib inhibitors prevent the binding of *CDK4/6* to D-type cyclin, thereby blocking the G1/S phase transition [59–61].

To determine the sensitivity of NB subtypes Cluster 1&2 and Cluster 3 to Palbociclib and Ribociclib inhibitors, we used OncoPredict tool [47] to predict the distribution of IC50 values for NB patients. Our results showed that the IC50 values of Palbociclib were consistently lower and significantly different in Cluster 3 compared to Cluster 1&2 (Figure 5B; see Materials and Methods). In contrast, Ribociclib had consistently higher IC50 values in Cluster 1&2 than in Cluster 3 (Figure 5B). Therefore, Palbociclib could be a potentially promising drug target for the treatment of Cluster 3, while Ribociclib may have an important therapeutic role for Clusters 1&2.

Expression suppression of MHC class II in myeloid cells drives poor prognosis in Cluster 3 subtype of NB

Based on the study conducted by Verhoeven et al. (2022) [5], we obtained a comprehensive single-cell dataset comprising 46,134 cells from 17 neuroblastoma (NB) donors (Figure 6A; Supplementary Table 9). This dataset encompasses 10 crucial immune cell types, including B cells, ILC3, Macrophages, mDC, Monocytes, NK cells, Plasma cells, Tcyto, Th, and Treg cells. Employing a pre-trained XGBoost model, we successfully predicted the subtypes of the 17 patients, namely Cluster 1&2 and Cluster 3. Out of these patients, 6 were classified as C1&2 subtype, while the remaining 11 were identified as Cluster 3 subtype (Figure 6B; Supplementary Table 9). By integrating the clinical information associated with these NB patients, we observed a distinct pattern among the subtypes. Cluster 3 subtype patients were predominantly situated in the high-risk INRG category and exhibited the INRGSS M stage (Figure 6C). In contrast, Cluster 1&2 subtype NB patients displayed a higher prevalence in the low-risk INRG category and were predominantly in the INRGSS L1 and L2 stages (Figure 6C). To investigate the molecular characteristics specific to the C1&2 and C3 subtypes in the NB patients, we scrutinized the cell cycle distribution. Notably, Cluster 3 subtype cells exhibited a pronounced accumulation in the G1 phase (53.48%), indicating an elevated proliferative capacity (Figure 6D). Additionally, the cytotoxicity scores of Cluster 1&2 subtype were significantly higher compared to those of Cluster 3, aligning with the features observed in the NB-TARGET bulk classification (Figures 3C and 6E). In terms of gene expression, *GREB1* emerged as the important distinctive gene feature in the C3 subtype, with the highest proportion of positive expression observed in Macrophages (Figure 6F). Abundance analysis across different cell types within the Cluster 1&2 and Cluster 3 subtypes demonstrated a substantial enrichment of Macrophages and Monocytes in Cluster 3, while Th cells exhibited a significantly higher abundance in Cluster 1&2 (Figure 6G).

To investigate the variations in cell-to-cell signaling and interactions between the Cluster 1&2 and Cluster 3 subtypes and gain insights into the unfavorable prognosis associated with the Cluster 3 subtype, we employed CellChat [48] for cell-cell interaction

analysis. Our findings revealed significantly stronger interactions between Macrophages, Monocytes, and Treg cells in the Cluster 1&2 subtype compared to the Cluster 3 subtype (Figure 6H, 6I). Further analysis of receptor and ligand genes highlighted a notable

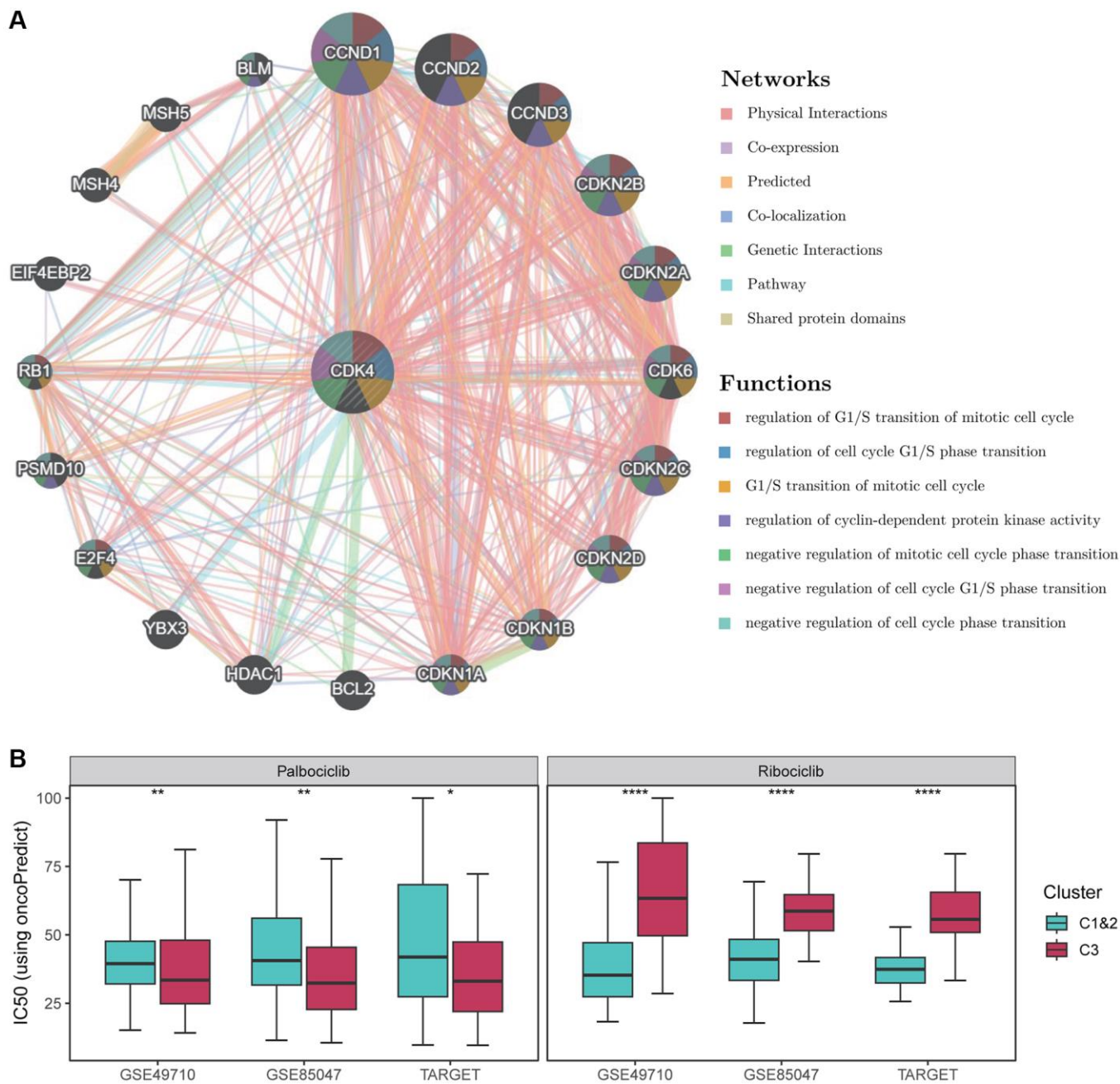


Figure 5. Drug sensitivity analysis of *CDK4* inhibitors. (A) Functional analysis of the protein-protein interaction network and *CDK4*, along with its neighboring genes. The edges of the network are color-coded to indicate the bioinformatics methods used, including physical interactions, co-expression, site prediction, co-localization, pathway and genetic interactions, and shared protein structural domains. The nodes of the network are also color-coded to reflect the enrichment results of the genome. The size of each circle corresponds to the rank of the gene associated with *CDK4*, while the width of each line represents the weight of the data source used in the composite network. (B) Box plots show the distribution of IC50 values for Palbociclib as well as Ribociclib in Fges-derived subtypes. *P*-values were obtained from *t*-tests. **p* < 0.05; ***p* < 0.01; *****p* < 0.0001.

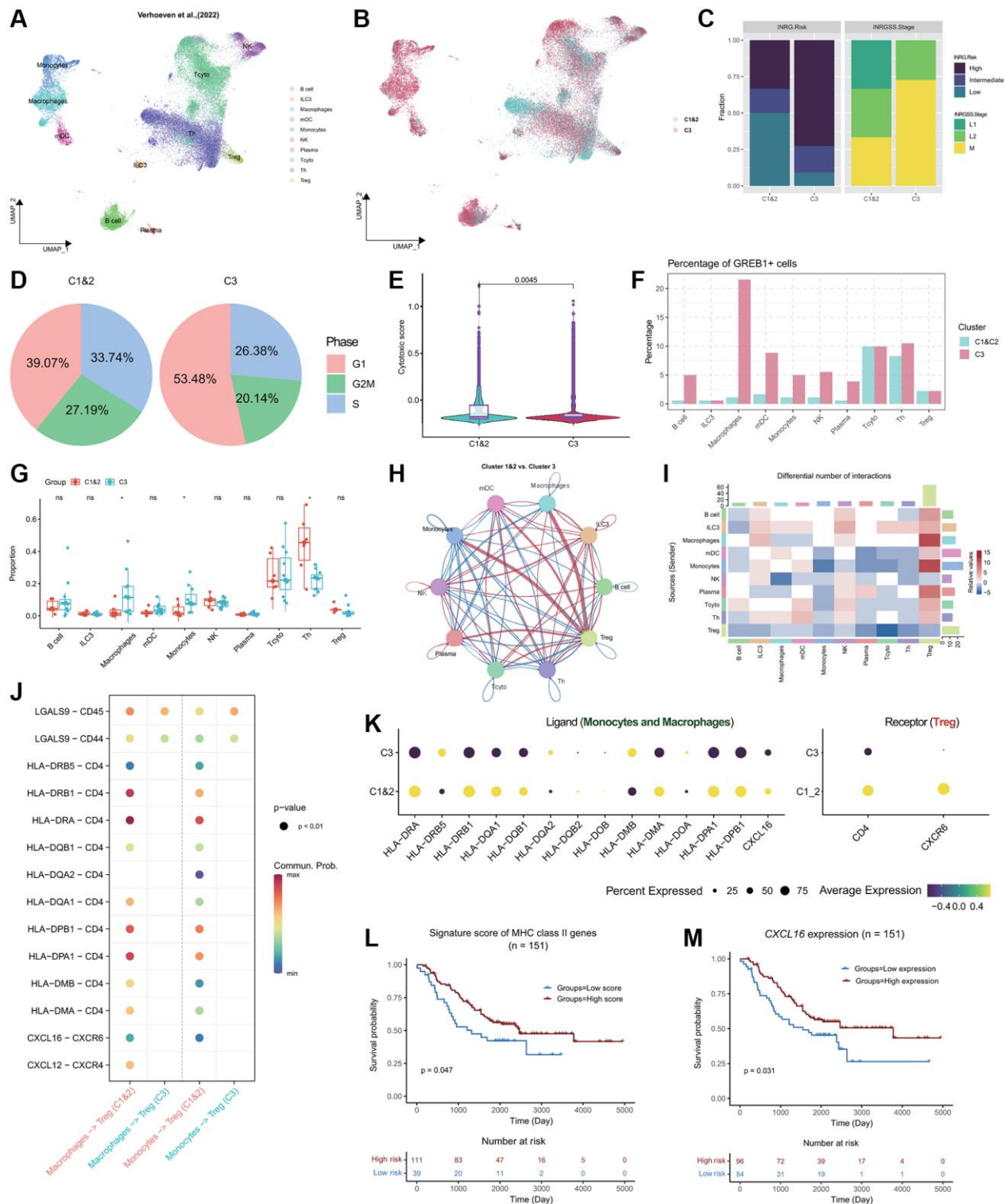


Figure 6. Single-cell profiling of the NB immune microenvironment and subtype-specific interactions. (A) Global overview of NB immune cell atlas containing 46,134 cells, color coded by annotated cell type ($n = 17$). (B) Global overview of NB immune cell atlas, color coded by predicted NB subtypes. (C) Stacked bar plots showing the distribution of Cluster 1&2 and Cluster 3 subtypes of NB patients in the INRG (left panel) and INRGSS (right panel) classifications. (D) Pie plots showing the percentage of cells in different NB subtypes in the G1, G2M, and S phases. (E) Violin plots combined with boxplots show the distribution of cytotoxic scores of cells in Cluster 1&2 and Cluster 3 subtypes. P -value was obtained from t -test. (F) Grouped bar plot showing the percentage of *GREB1*+ cells in different immune cell types of Cluster 1&2 and Cluster 3 patients. (G) Grouped boxplot showing the cellular proportion of Cluster 1&2 and Cluster 3 patients. P -values were obtained from t -tests. ns, not significant; * $p < 0.05$. (H) Interaction map depicting the ligand-receptor interactions within the NB immune microenvironment. Red indicates stronger p interactions between ligands and receptors in Cluster 1&2 compared to Cluster 3, while

blue indicates weaker interactions in Cluster 1&2 compared to Cluster 3. The thickness of the lines represents the strength of the differences. (I) Heatmap showing the differences in ligand-receptor interactions between Cluster 1&2 and Cluster 3. Red indicates stronger interactions between ligands and receptors in Cluster 1&2 compared to Cluster 3, while blue indicates weaker interactions in Cluster 1&2 compared to Cluster 3. (J) Bubble plot showing the significant interactions between receptor and ligand genes among Monocytes, Macrophages, and Treg cells in both Cluster 1&2 and Cluster 3 subtypes ($p < 0.01$). The color gradient ranging towards red indicates stronger interactions. (K) Bubble plot showing the expression of ligands MHC II molecules and *CXCL16* in Monocytes and Macrophages of both Cluster 1&2 and Cluster 3 subtypes, as well as the expression of receptor genes *CD4* and *CXCR6* in Treg cells. (L) KM curve showing the stratification derived by the signature score of MHC Class II genes exhibiting significant differences in prognosis. P -value was obtained by log-rank test. (M) KM curve showing the stratification derived by the expression of *CXCL16* exhibiting significant differences in prognosis. P -value was obtained by log-rank test.

deficiency in the interaction between MHC Class II molecules and *CD4* in Cluster 3, as well as the *CXCL16*-*CXCR6* axis interaction (Figure 6J). Additionally, Monocytes and Macrophages within the Cluster 3 subtype exhibited suppressed expression of MHC Class II genes and *CXCL16*, indicating an unfavorable prognosis for NB patients (Figure 6K–6M). In summary, our analysis emphasizes the down-regulation of MHC Class II and *CXCL16* expression in Monocytes and Macrophages within the Cluster 3 subtype, leading to weakened interactions with Treg cells and ultimately contributing to a poorer prognosis for patients with the Cluster 3 subtype.

DISCUSSION

NB is a childhood cancer that develops from immature nerve cells in the sympathetic nervous system. However, current clinical and molecular subtyping methods for NB have limitations, and may not always provide accurate prognostic information or guide treatment decisions [12, 62, 63]. This leads to challenges in predicting clinical outcomes and selecting appropriate treatments, highlighting the need for new approaches to better classify NB and improve disease management. To address this challenge, we explored the micro-environment of NB using Fges, which revealed some degree of heterogeneity that could potentially indicate subtypes. This speculation was supported when we performed consensus clustering of the Fges activity scores. Three subtypes (Cluster 1, Cluster 2, and Cluster 3) derived by Fges demonstrated significant differences in prognosis compared to the current mainstream NB subtypes (i.e., COG, and INSS) [9], providing a new strategy for NB typing.

By assessing the degree of immune infiltration, immunogenicity, CD8T cytotoxicity, and tumor purity of the Fges-derived three subtypes, we were able to shed light on their respective biological functions. Our analysis showed that Cluster 1 and Cluster 2 were more immunoreactive, while Cluster 3 demonstrated significantly higher tumor purity, which is consistent with its poor prognosis. Furthermore, gene ontology annotation and pathway analysis revealed that the three subtypes are associated with distinct biological

processes. Specifically, Cluster 1 is involved in immune activation, Cluster 2 is strongly associated with EMT, while Cluster 3 is enriched in biological processes or pathways such as cell cycle processes. It is important to note that previous studies [64–66] have shown a correlation between EMT activity and the ability of NB tumors to infiltrate and metastasize, ultimately, leading to worse prognosis. However, it is important to recognize that NB is a complex tumor and that different subtypes of NB may exhibit distinct biological features and clinical manifestations. Therefore, the prognostic impact of EMT activity may differ for different subtypes of NB. Additionally, further studies are necessary to investigate the role of EMT in the development and progression of NB.

To better extend Fges-derived subtypes in other NB cohorts, we developed a classification model using XGBoost to predict Cluster 1&2 versus Cluster 3. After evaluation, the model exhibited good performance in the training set (accuracy = 0.95). In the independent NB cohorts, the subtypes predicted by the classifier showed significant prognostic differences consistent with the expected pattern, which is crucial for investigating the Fges-derived subtypes in more extensive NB cohorts. Specifically, we found *GPR125*, *CDK4*, and *GREB1* to be the most significant marker genes in the Cluster 3 subtype. Our study suggests that these genes may play a crucial role in NB and that their over-expression or aberrant activation is closely associated with tumorigenesis, progression, and metastasis [54, 56, 66], and may be viable therapeutic targets for NB. Furthermore, our findings potentially shed light on the underlying reasons for the poor prognosis of Cluster 3. Given the significant impact of the *CD4K* gene on prognosis, we conducted further research on the drug guidance of *CD4K* inhibitors on Fges-derived subtypes, and found that Palbociclib was more sensitive in the Cluster 3, while Ribociclib performed well in the Cluster 1&2. This suggests that subtyping of NB may help in selecting appropriate treatment strategies to achieve better therapeutic effects.

In a separate single-cell analysis conducted on NB patients, we examined the characteristics and interactions among different subtypes. The study unveiled

unfavorable clinical prognostic features associated with the Cluster 3 subtype, including high-risk classification, increased proliferative capacity, and lower cytotoxicity scores. Moreover, compared to Cluster 1&2, the expression of MHC-II and *CXCL16* in monocytes and macrophages within Cluster 3 was suppressed, leading to weakened interactions with Treg cells, thus influencing patient prognosis. Specifically, Tregs, known for their immune regulatory role, typically interact with monocytes to maintain immune balance. However, the diminished interaction between monocytes presenting MHC class II molecules and *CD4* molecules in Tregs resulted in reduced suppressive effects by Tregs, leading to weakened immune regulation. Consequently, this could potentially trigger excessive or imbalanced immune responses, causing self-tissue damage or triggering a stronger immune response against tumor antigens. This could potentially result in excessive or imbalanced immune responses, causing damage to self-tissues or generating a stronger immune response against tumor antigens [67, 68]. These findings contribute significantly to our understanding of the differences between NB subtypes and the interactions among immune cells, offering valuable insights for the development of more effective treatment strategies.

Despite the promising results, our study has some limitations. Firstly, the study was based on a relatively small sample size, and more extensive validation is needed. Secondly, we only investigated two drugs, and more drugs need to be examined in future studies. Thirdly, further investigation is needed to validate the clinical utility of our subtyping approach. Nonetheless, our study highlights the potential of using Fges to derive novel subtypes of NB with significant differences in prognosis and treatment response. In conclusion, as research in NB subtyping and treatment strategies continues to advance, a multidisciplinary approach involving clinicians, researchers, and patients will be pivotal in translating these findings into more effective, personalized, and less burdensome treatment options. The ultimate goal is to enhance patient outcomes and the overall experience of those affected by NB.

AUTHOR CONTRIBUTIONS

YLY and DHZ designed the study. YYL, HYL, and HML did data analysis. YYL, HYL, XML and DHZ wrote and revised the manuscript. All authors contributed to and approved the final manuscript.

ACKNOWLEDGMENTS

Our gratitude goes out to all the authors who participated in this study and contributed to the data collection, coding, and manuscript writing.

CONFLICTS OF INTEREST

The authors declare no conflicts of interest related to this study.

FUNDING

This work was supported by The Shenzhen Science and Technology Program (SGDX20201103095404018), Shenzhen Fund for Guangdong Provincial High-Level Clinical Key Specialties (No. SZGSP012), Shenzhen Key Medical Discipline Construction Fund (No. SZXK034), Guangdong High-level Hospital Construction Fund, Shenzhen High-level Hospital Construction Fund, and “Jiangsu Funding Program for Excellent Postdoctoral Talent” (No. 2022ZB699), “Jiangsu Funding Program for Excellent Postdoctoral Talent” (No. 2022ZB699).

REFERENCES

1. Johnsen JI, Dyberg C, Wickström M. Neuroblastoma-A Neural Crest Derived Embryonal Malignancy. *Front Mol Neurosci.* 2019; 12:9. <https://doi.org/10.3389/fnmol.2019.00009> PMID:[30760980](https://pubmed.ncbi.nlm.nih.gov/30760980/)
2. Chennakesavalu M, Pudela C, Applebaum MA, Lee SM, Che Y, Naranjo A, Park JR, Volchenboum SL, Henderson TO, Cohn SL, Desai AV. Persistence of racial and ethnic disparities in risk and survival for patients with neuroblastoma over two decades. *EJC Paediatric Oncology.* 2023; 2:100022. <https://doi.org/10.1016/j.ejcped.2023.100022>
3. Henderson TO, Bhatia S, Pinto N, London WB, McGrady P, Crotty C, Sun CL, Cohn SL. Racial and ethnic disparities in risk and survival in children with neuroblastoma: a Children's Oncology Group study. *J Clin Oncol.* 2011; 29:76–82. <https://doi.org/10.1200/JCO.2010.29.6103> PMID:[21098321](https://pubmed.ncbi.nlm.nih.gov/21098321/)
4. Pinto NR, Applebaum MA, Volchenboum SL, Matthay KK, London WB, Ambros PF, Nakagawara A, Berthold F, Schleiermacher G, Park JR, Valteau-Couanet D, Pearson AD, Cohn SL. Advances in Risk Classification and Treatment Strategies for Neuroblastoma. *J Clin Oncol.* 2015; 33:3008–17. <https://doi.org/10.1200/JCO.2014.59.4648> PMID:[26304901](https://pubmed.ncbi.nlm.nih.gov/26304901/)
5. Verhoeven BM, Mei S, Olsen TK, Gustafsson K, Valind A, Lindström A, Gisselsson D, Fard SS, Hagerling C, Kharchenko PV, Kogner P, Johnsen JI, Baryawno N. The immune cell atlas of human neuroblastoma. *Cell Rep Med.* 2022; 3:100657. <https://doi.org/10.1016/j.xcrm.2022.100657> PMID:[35688160](https://pubmed.ncbi.nlm.nih.gov/35688160/)

6. Irwin MS, Naranjo A, Zhang FF, Cohn SL, London WB, Gastier-Foster JM, Ramirez NC, Pfau R, Reshmi S, Wagner E, Nuchtern J, Asgharzadeh S, Shimada H, et al. Revised Neuroblastoma Risk Classification System: A Report From the Children's Oncology Group. *J Clin Oncol*. 2021; 39:3229–41.
<https://doi.org/10.1200/JCO.21.00278>
PMID:[34319759](https://pubmed.ncbi.nlm.nih.gov/34319759/)
7. Castleberry RP, Pritchard J, Ambros P, Berthold F, Brodeur GM, Castel V, Cohn SL, De Bernardi B, Dicks-Mireaux C, Frappaz D, Haase GM, Haber M, Jones DR, et al. The International Neuroblastoma Risk Groups (INRG): a preliminary report. *Eur J Cancer*. 1997; 33:2113–6.
[https://doi.org/10.1016/s0959-8049\(97\)00202-5](https://doi.org/10.1016/s0959-8049(97)00202-5)
PMID:[9516864](https://pubmed.ncbi.nlm.nih.gov/9516864/)
8. Monclair T, Brodeur GM, Ambros PF, Brisse HJ, Cecchetto G, Holmes K, Kaneko M, London WB, Matthay KK, Nuchtern JG, von Schweinitz D, Simon T, Cohn SL, Pearson AD, and INRG Task Force. The International Neuroblastoma Risk Group (INRG) staging system: an INRG Task Force report. *J Clin Oncol*. 2009; 27:298–303.
<https://doi.org/10.1200/JCO.2008.16.6876>
PMID:[19047290](https://pubmed.ncbi.nlm.nih.gov/19047290/)
9. Sokol E, Desai AV. The Evolution of Risk Classification for Neuroblastoma. *Children (Basel)*. 2019; 6:27.
<https://doi.org/10.3390/children6020027>
PMID:[30754710](https://pubmed.ncbi.nlm.nih.gov/30754710/)
10. De Brouwer S, De Preter K, Kumps C, Zabrocki P, Porcu M, Westerhout EM, Lakeman A, Vandesompele J, Hoebeeck J, Van Maerken T, De Paepe A, Laureys G, Schulte JH, et al. Meta-analysis of neuroblastomas reveals a skewed ALK mutation spectrum in tumors with MYCN amplification. *Clin Cancer Res*. 2010; 16:4353–62.
<https://doi.org/10.1158/1078-0432.CCR-09-2660>
PMID:[20719933](https://pubmed.ncbi.nlm.nih.gov/20719933/)
11. Riobello C, López-Hernández A, Cabal VN, García-Marín R, Suárez-Fernández L, Sánchez-Fernández P, Vivanco B, Blanco V, López F, Franchi A, Llorente JL, Hermsen MA. IDH2 Mutation Analysis in Undifferentiated and Poorly Differentiated Sinonasal Carcinomas for Diagnosis and Clinical Management. *Am J Surg Pathol*. 2020; 44:396–405.
<https://doi.org/10.1097/PAS.0000000000001420>
PMID:[31876581](https://pubmed.ncbi.nlm.nih.gov/31876581/)
12. Wang LL, Sukanuma R, Ikegaki N, Tang X, Naranjo A, McGrady P, London WB, Hogarty MD, Gastier-Foster JM, Look AT, Park JR, Maris JM, Cohn SL, et al. Neuroblastoma of undifferentiated subtype, prognostic significance of prominent nucleolar formation, and MYC/MYCN protein expression: a report from the Children's Oncology Group. *Cancer*. 2013; 119:3718–26.
<https://doi.org/10.1002/cncr.28251>
PMID:[23901000](https://pubmed.ncbi.nlm.nih.gov/23901000/)
13. Ambros IM, Zellner A, Roald B, Amann G, Ladenstein R, Printz D, Gadner H, Ambros PF. Role of ploidy, chromosome 1p, and Schwann cells in the maturation of neuroblastoma. *N Engl J Med*. 1996; 334:1505–11.
<https://doi.org/10.1056/NEJM199606063342304>
PMID:[8618605](https://pubmed.ncbi.nlm.nih.gov/8618605/)
14. Taylor JS, Zeki J, Ornell K, Coburn J, Shimada H, Ikegaki N, Chiu B. Down-regulation of MYCN protein by CX-5461 leads to neuroblastoma tumor growth suppression. *J Pediatr Surg*. 2019; 54:1192–7.
<https://doi.org/10.1016/j.jpedsurg.2019.02.028>
PMID:[30879743](https://pubmed.ncbi.nlm.nih.gov/30879743/)
15. Wang LL, Teshiba R, Ikegaki N, Tang XX, Naranjo A, London WB, Hogarty MD, Gastier-Foster JM, Look AT, Park JR, Maris JM, Cohn SL, Seeger RC, et al. Augmented expression of MYC and/or MYCN protein defines highly aggressive MYC-driven neuroblastoma: a Children's Oncology Group study. *Br J Cancer*. 2015; 113:57–63.
<https://doi.org/10.1038/bjc.2015.188>
PMID:[26035700](https://pubmed.ncbi.nlm.nih.gov/26035700/)
16. van Limpt V, Schramm A, van Lakeman A, Sluis P, Chan A, van Noesel M, Baas F, Caron H, Eggert A, Versteeg R. The Phox2B homeobox gene is mutated in sporadic neuroblastomas. *Oncogene*. 2004; 23:9280–8.
<https://doi.org/10.1038/sj.onc.1208157>
PMID:[15516980](https://pubmed.ncbi.nlm.nih.gov/15516980/)
17. Javanmardi N, Fransson S, Djos A, Sjöberg RM, Nilsson S, Truvé K, Kogner P, Martinsson T. Low Frequency ALK Hotspots Mutations In Neuroblastoma Tumours Detected By Ultra-deep Sequencing: Implications For ALK Inhibitor Treatment. *Sci Rep*. 2019; 9:2199.
<https://doi.org/10.1038/s41598-018-37240-z>
PMID:[30778092](https://pubmed.ncbi.nlm.nih.gov/30778092/)
18. Hua Z, Gu X, Dong Y, Tan F, Liu Z, Thiele CJ, Li Z. PI3K and MAPK pathways mediate the BDNF/TrkB-increased metastasis in neuroblastoma. *Tumour Biol*. 2016; 37:16227–36.
<https://doi.org/10.1007/s13277-016-5433-z>
PMID:[27752996](https://pubmed.ncbi.nlm.nih.gov/27752996/)
19. Veschi V, Liu Z, Voss TC, Ozbun L, Gryder B, Yan C, Hu Y, Ma A, Jin J, Mazur SJ, Lam N, Souza BK, Giannini G, et al. Epigenetic siRNA and Chemical Screens Identify SETD8 Inhibition as a Therapeutic Strategy for p53 Activation in High-Risk Neuroblastoma. *Cancer Cell*. 2017; 31:50–63.
<https://doi.org/10.1016/j.ccell.2016.12.002>
PMID:[28073004](https://pubmed.ncbi.nlm.nih.gov/28073004/)
20. Capasso M, Diskin SJ, Totaro F, Longo L, De Mariano M, Russo R, Cimmino F, Hakonarson H, Tonini GP,

- Devoto M, Maris JM, Iolascon A. Replication of GWAS-identified neuroblastoma risk loci strengthens the role of BARD1 and affirms the cumulative effect of genetic variations on disease susceptibility. *Carcinogenesis*. 2013; 34:605–11.
<https://doi.org/10.1093/carcin/bgs380>
PMID:23222812
21. Godbout R, Packer M, Bie W. Overexpression of a DEAD box protein (DDX1) in neuroblastoma and retinoblastoma cell lines. *J Biol Chem*. 1998; 273:21161–8.
<https://doi.org/10.1074/jbc.273.33.21161>
PMID:9694872
22. Sausen M, Leary RJ, Jones S, Wu J, Reynolds CP, Liu X, Blackford A, Parmigiani G, Diaz LA Jr, Papadopoulos N, Vogelstein B, Kinzler KW, Velculescu VE, Hogarty MD. Integrated genomic analyses identify ARID1A and ARID1B alterations in the childhood cancer neuroblastoma. *Nat Genet*. 2013; 45:12–7.
<https://doi.org/10.1038/ng.2493>
PMID:23202128
23. Zhang L, Lv C, Jin Y, Cheng G, Fu Y, Yuan D, Tao Y, Guo Y, Ni X, Shi T. Deep Learning-Based Multi-Omics Data Integration Reveals Two Prognostic Subtypes in High-Risk Neuroblastoma. *Front Genet*. 2018; 9:477.
<https://doi.org/10.3389/fgene.2018.00477>
PMID:30405689
24. Bagaev A, Kotlov N, Nomie K, Svelkolkin V, Gafurov A, Isaeva O, Osokin N, Kozlov I, Frenkel F, Gancharova O, Almog N, Tsiper M, Ataullakhanov R, Fowler N. Conserved pan-cancer microenvironment subtypes predict response to immunotherapy. *Cancer Cell*. 2021; 39:845–65.e7.
<https://doi.org/10.1016/j.ccell.2021.04.014>
PMID:34019806
25. Fridman WH, Pagès F, Sautès-Fridman C, Galon J. The immune contexture in human tumours: impact on clinical outcome. *Nat Rev Cancer*. 2012; 12:298–306.
<https://doi.org/10.1038/nrc3245>
PMID:22419253
26. Garcia-Diaz A, Shin DS, Moreno BH, Saco J, Escuin-Ordinas H, Rodriguez GA, Zaretsky JM, Sun L, Hugo W, Wang X, Parisi G, Saus CP, Torrejon DY, et al. Interferon Receptor Signaling Pathways Regulating PD-L1 and PD-L2 Expression. *Cell Rep*. 2017; 19:1189–201.
<https://doi.org/10.1016/j.celrep.2017.04.031>
PMID:28494868
27. Wang X, Wang X, Xu M, Sheng W. Effects of CAF-Derived MicroRNA on Tumor Biology and Clinical Applications. *Cancers (Basel)*. 2021; 13:3160.
<https://doi.org/10.3390/cancers13133160>
PMID:34202583
28. Chaudhary RK, Khanal P, Mateti UV, Shastry CS, Shetty J. Identification of hub genes involved in cisplatin resistance in head and neck cancer. *J Genet Eng Biotechnol*. 2023; 21:9.
<https://doi.org/10.1186/s43141-023-00468-y>
PMID:36715825
29. Chaudhary RK, Patil P, Ananthesh L, Gowdru Srinivasa M, Mateti UV, Shetty V, Khanal P. Identification of signature genes and drug candidates for primary plasma cell leukemia: An integrated system biology approach. *Comput Biol Med*. 2023; 162:107090.
<https://doi.org/10.1016/j.combiomed.2023.107090>
PMID:37295388
30. Chaudhary RK, Patil P, Mateti UV, Alagundagi DB, Shetty V. Theranostic Potential of EFNB2 for Cetuximab Resistance in Head and Neck Cancer. *Indian J Otolaryngol Head Neck Surg*. 2023; 75:1923–36.
<https://doi.org/10.1007/s12070-023-03739-9>
PMID:37636764
31. Li H, Sharma A, Ming W, Sun X, Liu H. A deconvolution method and its application in analyzing the cellular fractions in acute myeloid leukemia samples. *BMC Genomics*. 2020; 21:652.
<https://doi.org/10.1186/s12864-020-06888-1>
PMID:32967610
32. Wang C, Gong B, Bushel PR, Thierry-Mieg J, Thierry-Mieg D, Xu J, Fang H, Hong H, Shen J, Su Z, Meehan J, Li X, Yang L, et al. The concordance between RNA-seq and microarray data depends on chemical treatment and transcript abundance. *Nat Biotechnol*. 2014; 32:926–32.
<https://doi.org/10.1038/nbt.3001>
PMID:25150839
33. Munro SA, Lund SP, Pine PS, Binder H, Clevert DA, Conesa A, Dopazo J, Fasold M, Hochreiter S, Hong H, Jafari N, Kreil DP, Łabaj PP, et al. Assessing technical performance in differential gene expression experiments with external spike-in RNA control ratio mixtures. *Nat Commun*. 2014; 5:5125.
<https://doi.org/10.1038/ncomms6125>
PMID:25254650
34. Su Z, Fang H, Hong H, Shi L, Zhang W, Zhang W, Zhang Y, Dong Z, Lancashire LJ, Bessarabova M, Yang X, Ning B, Gong B, et al. An investigation of biomarkers derived from legacy microarray data for their utility in the RNA-seq era. *Genome Biol*. 2014; 15:523.
<https://doi.org/10.1186/s13059-014-0523-y>
PMID:25633159
35. Rajbhandari P, Lopez G, Capdevila C, Salvatori B, Yu J, Rodriguez-Barrueco R, Martinez D, Yarmarkovich M,

- Weichert-Leahey N, Abraham BJ, Alvarez MJ, Iyer A, Harenza JL, et al. Cross-Cohort Analysis Identifies a TEAD4-MYCN Positive Feedback Loop as the Core Regulatory Element of High-Risk Neuroblastoma. *Cancer Discov.* 2018; 8:582–99.
<https://doi.org/10.1158/2159-8290.CD-16-0861>
PMID:[29510988](https://pubmed.ncbi.nlm.nih.gov/29510988/)
36. Davis S, Meltzer PS. GEOquery: a bridge between the Gene Expression Omnibus (GEO) and BioConductor. *Bioinformatics.* 2007; 23:1846–7.
<https://doi.org/10.1093/bioinformatics/btm254>
PMID:[17496320](https://pubmed.ncbi.nlm.nih.gov/17496320/)
37. Gautier L, Cope L, Bolstad BM, Irizarry RA. affy--analysis of Affymetrix GeneChip data at the probe level. *Bioinformatics.* 2004; 20:307–15.
<https://doi.org/10.1093/bioinformatics/btg405>
PMID:[14960456](https://pubmed.ncbi.nlm.nih.gov/14960456/)
38. Hänzelmann S, Castelo R, Guinney J. GSEA: gene set variation analysis for microarray and RNA-seq data. *BMC Bioinformatics.* 2013; 14:7.
<https://doi.org/10.1186/1471-2105-14-7>
PMID:[23323831](https://pubmed.ncbi.nlm.nih.gov/23323831/)
39. Wilkerson MD, Hayes DN. ConsensusClusterPlus: a class discovery tool with confidence assessments and item tracking. *Bioinformatics.* 2010; 26:1572–3.
<https://doi.org/10.1093/bioinformatics/btq170>
PMID:[20427518](https://pubmed.ncbi.nlm.nih.gov/20427518/)
40. Kassambara A, Kosinski M, Biecek P, Fabian S. Package ‘survminer’. Drawing Survival Curves using ‘ggplot2’ (R package version 03 1). 2017.
41. Stuart T, Butler A, Hoffman P, Hafemeister C, Papalexi E, Mauck WM 3rd, Hao Y, Stoeckius M, Smibert P, Satija R. Comprehensive Integration of Single-Cell Data. *Cell.* 2019; 177:1888–902.e21.
<https://doi.org/10.1016/j.cell.2019.05.031>
PMID:[31178118](https://pubmed.ncbi.nlm.nih.gov/31178118/)
42. Yu G, Wang LG, Han Y, He QY. clusterProfiler: an R package for comparing biological themes among gene clusters. *OMICS.* 2012; 16:284–7.
<https://doi.org/10.1089/omi.2011.0118>
PMID:[22455463](https://pubmed.ncbi.nlm.nih.gov/22455463/)
43. Yoshihara K, Shahmoradgoli M, Martínez E, Vegesna R, Kim H, Torres-García W, Treviño V, Shen H, Laird PW, Levine DA, Carter SL, Getz G, Stemke-Hale K, et al. Inferring tumour purity and stromal and immune cell admixture from expression data. *Nat Commun.* 2013; 4:2612.
<https://doi.org/10.1038/ncomms3612>
PMID:[24113773](https://pubmed.ncbi.nlm.nih.gov/24113773/)
44. Charoentong P, Finotello F, Angelova M, Mayer C, Efremova M, Rieder D, Hackl H, Trajanoski Z. Pan-cancer Immunogenomic Analyses Reveal Genotype-Immunophenotype Relationships and Predictors of Response to Checkpoint Blockade. *Cell Rep.* 2017; 18:248–62.
<https://doi.org/10.1016/j.celrep.2016.12.019>
PMID:[28052254](https://pubmed.ncbi.nlm.nih.gov/28052254/)
45. Wang G, Xu D, Zhang Z, Li X, Shi J, Sun J, Liu HZ, Li X, Zhou M, Zheng T. The pan-cancer landscape of crosstalk between epithelial-mesenchymal transition and immune evasion relevant to prognosis and immunotherapy response. *NPJ Precis Oncol.* 2021; 5:56.
<https://doi.org/10.1038/s41698-021-00200-4>
PMID:[34158591](https://pubmed.ncbi.nlm.nih.gov/34158591/)
46. Chen T, Guestrin C. Xgboost: A scalable tree boosting system. In: *Proceedings of the 22nd acm sigkdd international conference on knowledge discovery and data mining.* 2016; 2016:785–94.
47. Maeser D, Gruener RF, Huang RS. oncoPredict: an R package for predicting in vivo or cancer patient drug response and biomarkers from cell line screening data. *Brief Bioinform.* 2021; 22:bbab260.
<https://doi.org/10.1093/bib/bbab260>
PMID:[34260682](https://pubmed.ncbi.nlm.nih.gov/34260682/)
48. Jin S, Guerrero-Juarez CF, Zhang L, Chang I, Ramos R, Kuan CH, Myung P, Plikus MV, Nie Q. Inference and analysis of cell-cell communication using CellChat. *Nat Commun.* 2021; 12:1088.
<https://doi.org/10.1038/s41467-021-21246-9>
PMID:[33597522](https://pubmed.ncbi.nlm.nih.gov/33597522/)
49. Blavier L, Yang RM, DeClerck YA. The Tumor Microenvironment in Neuroblastoma: New Players, New Mechanisms of Interaction and New Perspectives. *Cancers (Basel).* 2020; 12:2912.
<https://doi.org/10.3390/cancers12102912>
PMID:[33050533](https://pubmed.ncbi.nlm.nih.gov/33050533/)
50. Park JA, Cheung NV. Targets and Antibody Formats for Immunotherapy of Neuroblastoma. *J Clin Oncol.* 2020; 38:1836–48.
<https://doi.org/10.1200/JCO.19.01410>
PMID:[32167865](https://pubmed.ncbi.nlm.nih.gov/32167865/)
51. Spina E, Simundza J, Incassati A, Chandramouli A, Kugler MC, Lin Z, Khodadadi-Jamayran A, Watson CJ, Cowin P. Gpr125 is a unifying hallmark of multiple mammary progenitors coupled to tumor latency. *Nat Commun.* 2022; 13:1421.
<https://doi.org/10.1038/s41467-022-28937-x>
PMID:[35302059](https://pubmed.ncbi.nlm.nih.gov/35302059/)
52. Wu Y, Chen W, Gong L, Ke C, Wang H, Cai Y. Elevated G-Protein Receptor 125 (GPR125) Expression Predicts Good Outcomes in Colorectal Cancer and Inhibits Wnt/ β -Catenin Signaling Pathway. *Med Sci Monit.* 2018; 24:6608–16.

- <https://doi.org/10.12659/MSM.910105>
PMID:[30231258](https://pubmed.ncbi.nlm.nih.gov/30231258/)
53. Aust G, Zhu D, Van Meir EG, Xu L. Adhesion GPCRs in Tumorigenesis. *Handb Exp Pharmacol*. 2016; 234:369–96.
https://doi.org/10.1007/978-3-319-41523-9_17
PMID:[27832497](https://pubmed.ncbi.nlm.nih.gov/27832497/)
54. Molenaar JJ, Ebus ME, Koster J, van Sluis P, van Noesel CJ, Versteeg R, Caron HN. Cyclin D1 and CDK4 activity contribute to the undifferentiated phenotype in neuroblastoma. *Cancer Res*. 2008; 68:2599–609.
<https://doi.org/10.1158/0008-5472.CAN-07-5032>
PMID:[18413728](https://pubmed.ncbi.nlm.nih.gov/18413728/)
55. Rader J, Russell MR, Hart LS, Nakazawa MS, Belcastro LT, Martinez D, Li Y, Carpenter EL, Attiyeh EF, Diskin SJ, Kim S, Parasuraman S, Caponigro G, et al. Dual CDK4/CDK6 inhibition induces cell-cycle arrest and senescence in neuroblastoma. *Clin Cancer Res*. 2013; 19:6173–82.
<https://doi.org/10.1158/1078-0432.CCR-13-1675>
PMID:[24045179](https://pubmed.ncbi.nlm.nih.gov/24045179/)
56. Martinez-Monleon A, Kryh Öberg H, Gaarder J, Berbegall AP, Javanmardi N, Djos A, Ussowicz M, Taschner-Mandl S, Ambros IM, Øra I, Sandstedt B, Beiske K, Ladenstein R, et al. Amplification of CDK4 and MDM2: a detailed study of a high-risk neuroblastoma subgroup. *Sci Rep*. 2022; 12:12420.
<https://doi.org/10.1038/s41598-022-16455-1>
PMID:[35859155](https://pubmed.ncbi.nlm.nih.gov/35859155/)
57. Rihani A, Vandesompele J, Speleman F, Van Maerken T. Inhibition of CDK4/6 as a novel therapeutic option for neuroblastoma. *Cancer Cell Int*. 2015; 15:76.
<https://doi.org/10.1186/s12935-015-0224-y>
PMID:[26225123](https://pubmed.ncbi.nlm.nih.gov/26225123/)
58. D'Oto A, Fang J, Jin H, Xu B, Singh S, Mullasseril A, Jones V, Abu-Zaid A, von Buttlar X, Cooke B, Hu D, Shohet J, Murphy AJ, et al. KDM6B promotes activation of the oncogenic CDK4/6-pRB-E2F pathway by maintaining enhancer activity in MYCN-amplified neuroblastoma. *Nat Commun*. 2021; 12:7204.
<https://doi.org/10.1038/s41467-021-27502-2>
PMID:[34893606](https://pubmed.ncbi.nlm.nih.gov/34893606/)
59. Georger B, Bourdeaut F, DuBois SG, Fischer M, Geller JI, Gottardo NG, Marabelle A, Pearson ADJ, Modak S, Cash T, Robinson GW, Motta M, Matano A, et al. A Phase I Study of the CDK4/6 Inhibitor Ribociclib (LEE011) in Pediatric Patients with Malignant Rhabdoid Tumors, Neuroblastoma, and Other Solid Tumors. *Clin Cancer Res*. 2017; 23:2433–41.
<https://doi.org/10.1158/1078-0432.CCR-16-2898>
PMID:[28432176](https://pubmed.ncbi.nlm.nih.gov/28432176/)
60. Tripathy D, Bardia A, Sellers WR. Ribociclib (LEE011): Mechanism of Action and Clinical Impact of This Selective Cyclin-Dependent Kinase 4/6 Inhibitor in Various Solid Tumors. *Clin Cancer Res*. 2017; 23:3251–62.
<https://doi.org/10.1158/1078-0432.CCR-16-3157>
PMID:[28351928](https://pubmed.ncbi.nlm.nih.gov/28351928/)
61. Johnsen JI, Dyberg C, Fransson S, Wickström M. Molecular mechanisms and therapeutic targets in neuroblastoma. *Pharmacol Res*. 2018; 131:164–76.
<https://doi.org/10.1016/j.phrs.2018.02.023>
PMID:[29466695](https://pubmed.ncbi.nlm.nih.gov/29466695/)
62. Øra I, Eggert A. Progress in treatment and risk stratification of neuroblastoma: impact on future clinical and basic research. *Semin Cancer Biol*. 2011; 21:217–28.
<https://doi.org/10.1016/j.semcancer.2011.07.002>
PMID:[21798350](https://pubmed.ncbi.nlm.nih.gov/21798350/)
63. Acosta S, Lavarino C, Paris R, Garcia I, de Torres C, Rodríguez E, Beleta H, Mora J. Comprehensive characterization of neuroblastoma cell line subtypes reveals bilineage potential similar to neural crest stem cells. *BMC Dev Biol*. 2009; 9:12.
<https://doi.org/10.1186/1471-213X-9-12>
PMID:[19216736](https://pubmed.ncbi.nlm.nih.gov/19216736/)
64. Puram SV, Tirosh I, Parikh AS, Patel AP, Yizhak K, Gillespie S, Rodman C, Luo CL, Mroz EA, Emerick KS, Deschler DG, Varvares MA, Mylvaganam R, et al. Single-Cell Transcriptomic Analysis of Primary and Metastatic Tumor Ecosystems in Head and Neck Cancer. *Cell*. 2017; 171:1611–24.e24.
<https://doi.org/10.1016/j.cell.2017.10.044>
PMID:[29198524](https://pubmed.ncbi.nlm.nih.gov/29198524/)
65. Li H, Courtois ET, Sengupta D, Tan Y, Chen KH, Goh JI, Kong SL, Chua C, Hon LK, Tan WS, Wong M, Choi PJ, Wee LJK, et al. Reference component analysis of single-cell transcriptomes elucidates cellular heterogeneity in human colorectal tumors. *Nat Genet*. 2017; 49:708–18.
<https://doi.org/10.1038/ng.3818>
PMID:[28319088](https://pubmed.ncbi.nlm.nih.gov/28319088/)
66. Dong R, Yang R, Zhan Y, Lai HD, Ye CJ, Yao XY, Luo WQ, Cheng XM, Miao JJ, Wang JF, Liu BH, Liu XQ, Xie LL, et al. Single-Cell Characterization of Malignant Phenotypes and Developmental Trajectories of Adrenal Neuroblastoma. *Cancer Cell*. 2020; 38:716–33.e6.
<https://doi.org/10.1016/j.ccell.2020.08.014>
PMID:[32946775](https://pubmed.ncbi.nlm.nih.gov/32946775/)
67. Wardell CM, MacDonald KN, Levings MK, Cook L. Cross talk between human regulatory T cells and antigen-presenting cells: Lessons for clinical applications. *Eur J Immunol*. 2021; 51:27–38.

<https://doi.org/10.1002/eji.202048746>

PMID:[33301176](https://pubmed.ncbi.nlm.nih.gov/33301176/)

68. Taams LS, van Amelsfort JM, Tiemessen MM, Jacobs KM, de Jong EC, Akbar AN, Bijlsma JW, Lafeber FP. Modulation of monocyte/macrophage function by human CD4+CD25+ regulatory T cells. *Hum Immunol.* 2005; 66:222–30.

<https://doi.org/10.1016/j.humimm.2004.12.006>

PMID:[15784460](https://pubmed.ncbi.nlm.nih.gov/15784460/)

SUPPLEMENTARY MATERIALS

Supplementary Tables

Please browse Full Text version to see the data of Supplementary Tables 1–3 and 5–7.

Supplementary Table 1. Summary of NB Cohorts used in the present study.

Supplementary Table 2. List of knowledge-based Functional Gene Expression Signatures (Fges).

Supplementary Table 3. Activity score of Fges in TARGET-NB cohort.

Supplementary Table 4. Prognostic effect of Fges activity scores in TARGET-NB cohort.

	HR	P-value
MHCI	1.821275179	0.039615164
MHCII	0.583836443	0.03041356
Coactivation_molecules	1.860932833	0.043129543
Effector_cells	0.636452651	0.13882156
T_cell_traffic	0.69708204	0.122197637
NK_cells	0.571949912	0.030198616
T_cells	0.634409842	0.078006928
B_cells	2.391219091	0.090508321
M1_signatures	0.723246517	0.163329204
Th1_signature	0.701370599	0.135638806
Antitumor_cytokines	0.50783405	0.032018353
Checkpoint_inhibition	0.51236251	0.024542153
Treg	0.489392939	0.002301173
T_reg_traffic	0.461730268	0.00401174
Neutrophil_signature	0.558161447	0.064353074
Granulocyte_traffic	0.664911796	0.085467705
MDSC	0.539404379	0.01864849
MDSC_traffic	0.556755849	0.028336472
Macrophages	0.712436722	0.149556066
Macrophage_DC_traffic	0.646581481	0.066628528
Th2_signature	0.60954905	0.086528464
Protumor_cytokines	1.761820619	0.015157943
CAF	1.674823647	0.06215062
Matrix	0.66364449	0.100221482
Matrix_remodeling	2.429286849	0.009150648
Angiogenesis	2.089288111	0.111961105
Endothelium	0.793468888	0.369515344
Proliferation_rate	2.803623103	0.000405439
EMT_signature	2.229806924	0.083548746

Supplementary Table 5. Consensus clustering results of TARGET-NB cohort based on the FGES activity score.

Supplementary Table 6. Differentially expressed genes among Fges-derived subtypes.

Supplementary Table 7. Gene ontology analysis results of Fges-derived subtypes.

Supplementary Table 8. List of features used for training XGBoost model.

hgnc_symbol	ensembl_gene_id	chromosome_name	start_position	end_position	description
GPR125	ENSG00000152990	4	22345071	22516066	adhesion G protein-coupled receptor A3 [Source:HGNC Symbol;Acc:HGNC:13839]
AHR	ENSG00000106546	7	16916359	17346152	aryl hydrocarbon receptor [Source:HGNC Symbol;Acc:HGNC:348]
CCL13	ENSG00000181374	17	34356480	34358610	C-C motif chemokine ligand 13 [Source:HGNC Symbol;Acc:HGNC:10611]
CCNB2	ENSG00000157456	15	59105126	59125045	cyclin B2 [Source:HGNC Symbol;Acc:HGNC:1580]
CD2	ENSG00000116824	1	116754430	116769229	CD2 molecule [Source:HGNC Symbol;Acc:HGNC:1639]
CD22	ENSG00000012124	19	35319261	35347361	CD22 molecule [Source:HGNC Symbol;Acc:HGNC:1643]
CD3E	ENSG00000198851	11	118304730	118316175	CD3 epsilon subunit of T-cell receptor complex [Source:HGNC Symbol;Acc:HGNC:1674]
CD52	ENSG00000169442	1	26317958	26320523	CD52 molecule [Source:HGNC Symbol;Acc:HGNC:1804]
CD79A	ENSG00000105369	19	41877279	41881372	CD79a molecule [Source:HGNC Symbol;Acc:HGNC:1698]
CDK4	ENSG00000135446	12	57747727	57756013	cyclin dependent kinase 4 [Source:HGNC Symbol;Acc:HGNC:1773]
CEBPD	ENSG00000221869	8	47736913	47738164	CCAAT enhancer binding protein delta [Source:HGNC Symbol;Acc:HGNC:1835]
CENPF	ENSG00000117724	1	214603185	214664574	centromere protein F [Source:HGNC Symbol;Acc:HGNC:1857]
CKM	ENSG00000104879	19	45306413	45322875	creatine kinase, M-type [Source:HGNC Symbol;Acc:HGNC:1994]
COL11A1	ENSG00000060718	1	102876467	103108872	collagen type XI alpha 1 chain [Source:HGNC Symbol;Acc:HGNC:2186]
CPNE7	ENSG00000178773	16	89575758	89597246	copine 7 [Source:HGNC Symbol;Acc:HGNC:2320]
CXCL10	ENSG00000169245	4	76021118	76023497	C-X-C motif chemokine ligand 10 [Source:HGNC Symbol;Acc:HGNC:10637]
FCER2	ENSG00000104921	19	7688758	7702146	Fc epsilon receptor II [Source:HGNC Symbol;Acc:HGNC:3612]
FAIM3	ENSG00000162894	1	206903317	206923247	Fc mu receptor [Source:HGNC Symbol;Acc:HGNC:14315]
FN1	ENSG00000115414	2	215360440	215436073	fibronectin 1 [Source:HGNC Symbol;Acc:HGNC:3778]
FOSB	ENSG00000125740	19	45467995	45475179	FosB proto-oncogene, AP-1 transcription factor subunit [Source:HGNC Symbol;Acc:HGNC:3797]
FOXD3	ENSG00000187140	1	63322567	63325128	forkhead box D3 [Source:HGNC Symbol;Acc:HGNC:3804]
GADD45B	ENSG00000099860	19	2476122	2478259	growth arrest and DNA damage inducible beta [Source:HGNC Symbol;Acc:HGNC:4096]
GREB1	ENSG00000196208	2	11482341	11642788	growth regulating estrogen receptor binding 1 [Source:HGNC Symbol;Acc:HGNC:24885]

HMOX1	ENSG00000100292	22	35380361	35394214	heme oxygenase 1 [Source:HGNC Symbol;Acc:HGNC:5013]
HP	ENSG00000257017	16	72054505	72061055	haptoglobin [Source:HGNC Symbol;Acc:HGNC:5141]
IGFBP1	ENSG00000146678	7	45888360	45893660	insulin like growth factor binding protein 1 (Source:HGNC Symbol;Acc:HGNC:5469)
ITGA8	ENSG00000077943	10	15513954	15719922	integrin subunit alpha 8 [Source:HGNC Symbol;Acc:HGNC:6144]
KLF4	ENSG00000136826	9	107484852	107490482	KLF transcription factor 4 [Source:HGNC Symbol;Acc:HGNC:6348]
LCK	ENSG00000182866	1	32251244	32286165	LCK proto-oncogene, Src family tyrosine kinase [Source:HGNC Symbol;Acc:HGNC:6524]
LGI4	ENSG00000153902	19	35124513	35142451	leucine rich repeat LGI family member 4 [Source:HGNC Symbol;Acc:HGNC:18712]
FAM60A	ENSG00000139146	12	31280584	31327058	SIN3-HDAC complex associated factor [Source:HGNC Symbol;Acc:HGNC:30702]
C8orf4	ENSG00000176907	8	40153482	40155310	transcriptional and immune response regulator [Source:HGNC Symbol;Acc:HGNC:1357]

Supplementary Table 9. Clinical and subtyping information of 19 NB single-cell datasets.

Sample. ID	Age. at. sampling	Risk. group. INRG. at. diagnosis	Stage. INRGSS.	Predict
NB01	4	Low	L1	C1&2
NB02	18	Intermediate	L2	C3
NB09	82	High	M	C3
NB11	138	Intermediate	L2	C1&2
NB12	101	High	M	C3
NB13	48	High	M	C3
NB15	76	High	M	C1&2
NB16	23	High	L2	C3
NB17	63	High	M	C1&2
NB18	111	High	M	C3
NB19	6	Low	L2	C3
NB20	83	High	M	C3
NB23	7	Intermediate	M	C3
NB24	128	High	M	C3
NB26	4	Low	L1	C1&2
NB34	100	High	M	C3
NB37	60	Low	L2	C1&2